Indian Journal of Fundamental and Applied Life Sciences ISSN: 2231– 6345 (Online)
An Open Access, Online International Journal Available at www.cibtech.org/sp.ed/jls/2014/04/jls.htm
2014 Vol. 4 (S4), pp. 758-768/Akbari et al.
Research Article

SUBSURFACE TARGETS IMAGING WITH AN IMPROVED BACK-PROJECTION ALGORITHM

Alireza Akbari[1], *Mirsattar Meshinchi-Asl[1], Mohmmad-Ali Riyahi[2]
[1] *Department of Geophysics, Science and Research Branch, Islamic Azad University, Tehran, Iran*
[2] *Institute of Geophysics, University of Tehran, Tehran, Iran*
**Author for Correspondence*

ABSTRACT
In ground penetrating radar (GPR) imaging, a single point target appears as a hyperbolic curve in the space-time image. In order to focus the hyperbolic curves in GPR images, first, the back-projection (BP) imaging algorithm was introduced. This standard BP imaging algorithm, was accompanied by a lot of artifacts, which have adverse effects on targets detection. Second, an improved BP imaging algorithm, based on cross-correlation between received signals for suppression artifacts, was proposed here. Third, to improve the quality of BP imaging algorithm, a weight factor was designed by analyzing the statistical character of receiving data for each point in regions of imaging. This proposed algorithm was applied on the simulation and the real GPR data and the results showed that the proposed BP imaging algorithm has superior suppression artifacts and produces images with high quality and resolution. In order to quantitatively describe the imaging results on the effect of artifact suppression, focusing parameter was evaluated.

Keywords: *GPR, Back-Projection, Algorithm, Imaging*

INTRODUCTION
GPR is an important nondestructive remote sensing tool that has been used in both military and civilian fields. Recently, GPR imaging has attracted lots of attention in detection of subsurface shallow small targets such as landmines and Unexploded Ordnance and also imaging behind the wall for security applications (Daniels, 2004; Carin, *et al.*, 1999) Depending on the application, different scanning schemes, namely, A-scan, B-scan, and C-scan, are employed (Daniels, 2004). The static measurement of the data collected at a single point is called an A-scan (Daniels, 2004). In the B-scan measurement situation, a downward looking GPR antenna is moved along a straight path on the top of the surface while the GPR sensor is collecting and recording the scattered field at different spatial positions. The GPR can either be bistatic with either a transmitted and receiver antenna or monostatic with a single transmitted and receiver antenna. For the monostatic arrangement in the space-time GPR image, a single point target appears as a hyperbolic curve because of the different trip times of the EM wave when the radar moves along a synthetic aperture and collects reflectivity of the subsurface targets (Ozdemir, *et al.*, 2004). With this hyperbolic curve, the resolution along the synthetic aperture direction shows undesired low resolution features owing to the tails of hyperbola. However, highly accurate information about the size, electromagnetic (EM) reflectivity, and depth of the buried objects is essential in most GPR applications. Therefore hyperbolic curve behavior in the space-time GPR image is often willing to be transformed to a focused pattern showing the object's true location and size together with its EM scattering.
The resolution along the depth achieved by the change of the transmitted signal’s frequency. The resolution along the direction of recording data is attained by the synthetic processing of the received data collected at different spatial points of the B-scan. While a fine resolution in the depth axis is usually easy to get by utilizing a broadband transmitted signal, the resolution along the scanning direction is much harder to realize and requires special treatment. For this purpose, many image focusing algorithms have been developed recently. Synthetic aperture imaging methods used in GPR applications can be sorted into two main categories; the back-propagation and the back-projection methods. The first group is formulated through various algorithms including the phase-shift method (Gazdag, 1978), the finite-difference method (Claerbout, 1972) and the frequency-wavenumber algorithm (Ozdemir *et al.*, 2008). The second group is

formulated through the geometrical approach and includes the diffraction summation (Miller *et al.*, 1978*)* and the back-projection (Carin *et al.*, 1999) algorithms. The principle of back-projection algorithm is very similar to the confocal microwave imaging (CMI) technique that employs Delay-And-Sum (DAS) algorithm was proposed for medical application (Fear *et al.*, 2002; Lim *et al.*, 2008). The idea of DAS algorithm is to sum all data coherency of points in regions of imaging at a time and repeat for all desired points (Gu *et al.*, 2004).

The common goal in a typical GPR image is to display the information of the spatial location and the reflectivity of an underground object. Therefore, the main challenge of GPR imaging technique is to devise an image reconstruction algorithm that provides high resolution and good suppression of strong artifacts and noise. In this paper, at first, the standard back-projection algorithm that was adapted to GPR imaging applications used for the image reconstruction.

The standard BP algorithm was limited with against strong noise and a lot of artifacts, which have adverse effects on the following work like detection targets. Thus, an improved BP is based on cross-correlation between the receiving signals proposed for decreasing noises and suppression artifacts. To improve the quality of the results of proposed BP imaging algorithm, a weight factor was designed for each point in region imaging. Compared to a standard BP algorithm scheme, the improved algorithm produces images of higher quality and resolution.

The proposed improved BP algorithm was applied to numerically generated GPR data and real B-scan GPR images, and the resultant focused GPR images were presented. In order to quantitatively describe the imaging result on the effect of suppression artifacts, a focusing parameter was evaluated.

Standard BP Algorithm Method

The 2-D imaging configuration of monostatic GPR is shown in Figure 1. The region of imaging is divided into two regions by z=0. The upper region is the air and characterized by permittivity $\epsilon_1 = \epsilon_0$ and permeability$\mu_1 = \mu_0$, where ϵ_0 and μ_0 denote permittivity and permeability in air, respectively. The lower region is the ground and characterized with homogeneous soil with relative permittivity $\epsilon_2 = \epsilon_r$ and relative permeability$\mu_2 = \mu_0$. For the sake of simplicity, we assumed that the conductivity in air and homogeneous soil is zero. In this monostatic GPR system, the antenna is located at $(y_a, -h)$ and synthesize an aperture on a line parallel to y axis at the distance h, with element M. The whole scanning length of targets is $y_b - y_a$. As the transmitter/receiver antenna pair moves along the synthetic aperture line $z = -h$ with the interval Δy, backscattering signals at the each focal aperture point $y_A = y_a + (i-1)\Delta y$, that $i = 1, 2, \dots M$, can be collected. The currently concerned antenna position in the monostatic GPR array is shown by black triangle with the sequence number i, whose coordinate is $(y_i, -h)$, while other M-1 antenna position are represented by white triangles.

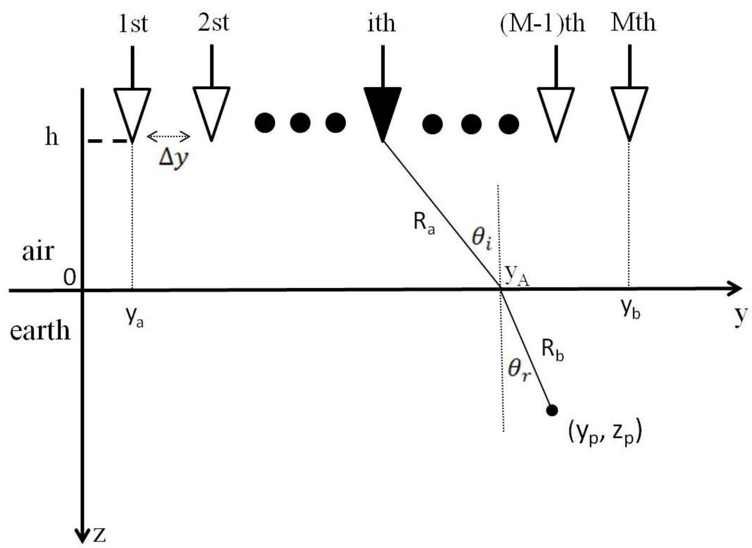

Figure 1: Imaging configuration

The regions of imaging are illuminated with a broadband signal $s(t)$. In the case of single point target p is located at $X_p = (y_p, z_p)$ and complex reflectivity $a(X_p)$, As shown in Figure (1), the received reflectivity of the i^{th} receiver is given by Equation 1:

$$p(y_i, t) = a(X_p)s(t - \tau_{pi}) \qquad (1)$$

Where, τ_{pi} is propagation delay as the EM wave travels from i^{th} transmitter to the focal point target located at $X_p = (y_p, z_p)$ and backs to the i^{th} receiver, as shown in Equation 2:

$$\tau_{p,i} = \frac{2R_a}{c} + \frac{2R_b}{v} \qquad (2)$$

Where, c and v represent, respectively, the propagation velocities of EM wave in air and soil, that $v = \frac{c}{\sqrt{\epsilon_r}}$, and$R_a$, and R_b are distances from the refraction point on the ground surface to transmitter/receiver pair point $(y_i, -h)$ and focal point (y_p, z_p).
The output of the i^{th} receiver of the whole region of imaging D is given by Equation 3:

$$P_D(y_i, t) = \iint_D p(y_i, t)dydz \qquad (3)$$

This process is repeated until all M transmitter/receiver position making a synthetic aperture are used sequentially. Thus, the output of all of the M transmitter/receiver position for formation of imaging result is as follows in Equation 4:

$$I(X) = \sum_{i=1}^{M} P_D(y_i, t) \qquad (4)$$

Research Article

This is the equation of standard BP imaging algorithm. Repetition of the process until all of the points in regions of imaging is calculated and forms image.

Improved Proposed Bp Algorithm

Modified Cross-Correlation BP

One of the disadvantages of the introduced standard BP imaging algorithm is that the level of energy of artifacts and noises in the imaging results is high. The existence of noises and artifacts decreases the contrast between objects and other things in imaging results. In order to decrease and suppress these noises and artifacts (Zetik *et al.*, 2005) and Foo and Kashyap (2004) have utilized a version of BP algorithm using cross-correlation of received signals. However, that BP imaging algorithm needs an additional reference channel to correlate with receiving signals. The position of reference channel should be located away from the center of transmitter/receiver array and reference signal should be collected there. This means that addition hardware receiver and signal processing procedure should be added.

In fact, more information can be obtained from the original receiving signal. Based on cross-correlation for decreasing the noises and suppressing the artifacts, an improved BP algorithm for GPR application was proposed. At this kind of improved algorithm, the response of the single point p will not be summed directly as Equation 4. Instead, similar CMI method (Lim *et al.*, 2008). We will first calculate the cross-correlation of values between responses of focal point p in M transmitter/receiver position and then summation is made to take the imaging result of point P as follows:

$$I(X) = \sum_{i=1}^{M-1} \sum_{j=i+1}^{M} P_D(y_i, t).P_D(y_j, t) \qquad (5)$$

By this additional step, noises and artifacts in imaging result will be suppressed effectively.

Design Weight Factor

The value of standard deviation and mean of 2D GPR data that containing buried target reflected waves are greater than the 2D GPR data that do not contain buried target reflected waves (Mast and Johansson, 1994). So, the ratio of the mean value to the standard deviation of focal point target is much bigger than corresponding value of the other focal points, where there are no real targets. Thus, the standard BP imaging algorithm can be modified by this characteristic.

By charactering a weight factor $\omega(y_n, z_m)$, the result of the imaging quality can be improved using mean (6) and standard deviation (7).

$$m = \frac{\sum_{i=1}^{M} e_{p,i}}{M} \qquad (6)$$

$$\upsilon = \left\{\frac{1}{M}\sum_{i=1}^{M}\left(e_{p,i} - m\right)^2\right\}^{\frac{1}{2}} \qquad (7)$$

The weighting factor can be designed as follows:

$$\omega(y_n, z_m) = \begin{cases} 1 & \upsilon = 0 \\ \dfrac{m}{\upsilon} & elsewhere \end{cases} \qquad (8)$$

Now, the final improved proposed BP imaging algorithm is obtained as Equation 9:

$$E_p = \omega(y_n, z_m) \sum_{i=1}^{M-1} \sum_{j=i+1}^{M} P_D(y_i, t).P_D(y_j, t) \qquad (9)$$

The Implementation of the Algorithm

The steps of implementation of the improved proposed BP imaging algorithm can be expressed as follows:

1- Calculate the round-trip time delays from M antenna position to focal point p and form $\{\tau_{p,1}, \tau_{p,2}, \dots, \tau_{p,M}\}$.

2- Calculate the response point P in all the M receiving signal $s_i(t)$ and form $\{e_{p,1}, e_{p,2}, \dots, e_{p,M}\}$ that $e_{p,i} = s_i(t)|_{t=\tau_{p,i}}$.

3- For the standard BP algorithm, a summation is made to take the imaging result for focal point p as follow (10):

$$E_p = \sum_{i=1}^{M} e_{p,i} \qquad (10)$$

4- For improved BP imaging algorithm, calculate cross-correlation to utilize the relativities between M receiving signal as follows (11):

$$E_p = \sum_{i=1}^{M-1} \sum_{j=i+1}^{M} e_{p,i} \cdot e_{p,j} \qquad (11)$$

5- The weighting factor $\omega(y_n, z_m)$ is calculated for focal point p.

6- The final result of focal point p in the improved BP imaging algorithm can be taking with (12):

$$E_p = \omega(y_n, z_m) \sum_{i=1}^{M-1} \sum_{j=i+1}^{M} e_{p,i} \cdot e_{p,j} \qquad (12)$$

7- Repeat the steps up to cover all of points in regions of imaging.

Simulation and Experiments Results

The validity and effectiveness of proposed BP algorithm were tested via simulated and real measured data.

Simulation Results

In this section, we describe the EM computer model that closely simulates the operation of GPR for underground target detection. This model uses the Finite Difference Time Domain (FDTD) method for EM field calculation. A simulation consists of exciting one transmitter with current pulse and receiving the time domain y component of the electric field at the receiver location. This simulates a mono-static radar configuration and is repeated separately for each transmitter/receiver pair.

The received signal includes the wave propagation directly between the transmitter and receiver, the EM wave reflected by air-ground interface, and EM wave scattered by underground anomaly. Since we are interested only received signal from buried target, we should cancel the direct and interface reflected signals. Here, by using a monostatic arrangement, the direct wave was cancelled and for removing the air-ground interface reflected signals, mean subtracted method was used (Foo and Kashyap, 2004).

For the EM calculation of scattering from underground region, a CST microwave imaging simulator was employed. This simulator can successfully estimate EM scattering for any medium and all targets that are buried there by FDTD method.

The backscattered EM signature was collected along synthetic aperture in y direction for a total of 61 discrete spatial points. The distance between two antenna positions was equal to 5 cm. The antennas are placed at 5 cm above air-ground interface. The entire synthetic aperture was 3.05 m along y dimension. The frequency was varied from 1 to 4 GHz with a 2.5 GHz central frequency. Three landmines with identical size were located at different locations as the buried targets. These landmines, with 12 cm in diameter and 6 cm in length, were put horizontally at (-0.7,-0.5), (-0.50,-0.2) and (-0.7, 0.2) in meters. These landmines were buried in depths 10cm, 5cm, and 15cm, respectively. This targets were buried in homogeneous soil with the dielectric constant$\epsilon_r = 13$. This dielectric property is the characteristic of wet sandy soil. The mono-static GPR arrangement geometry and three landmines positions are shown in Figure 2(a) and (b).

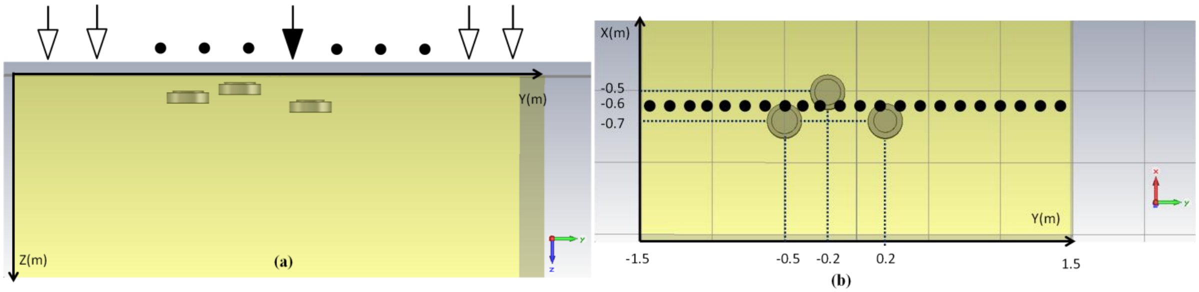

Figurer 2: Simulated GPR arrangement geometry for three landmines. (a) Three landmines buried in wet sandy soil. (b) Projection on the $x - y$ plane.

Each landmine displays its hyperbola shaped range profiles as radar approaches and then eventually passes each target. In addition to the main response from each landmine, there is some late time responses, which are generated from wave travelling around the body of landmine.

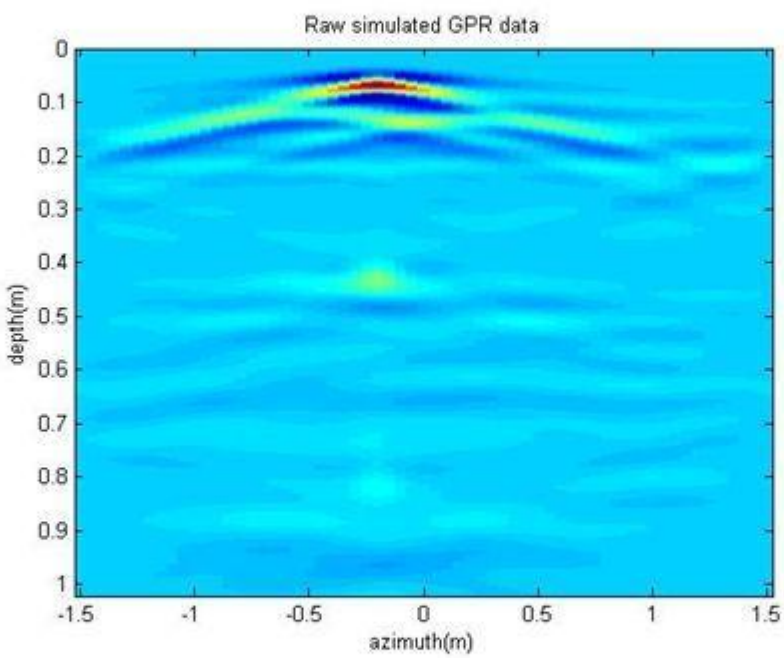

Figure 3: Raw simulated GPR data after preprocessing

As presented in Figure 3, the traditional GPR image was obtained in 2D spatial-time backscattered data after removing air-ground interface effect by mean subtracted method. As expected, the image was hyperbolically defocused due to different round-trip distances between targets and antennas while radar is moving along straight line for the monostatic arrangement.

For focusing hyperbolas, due to the buried landmines, the standard and the proposed improved algorithms were applied and images results from standard BP algorithm and improved BP algorithm are shown in Figure 4. It is obvious that Figure 4(a) has much more noise and artifacts than Figure 4(b). Therefore, the proposed improved BP imaging algorithm can obtain a better imaging result with a good artifacts suppression.

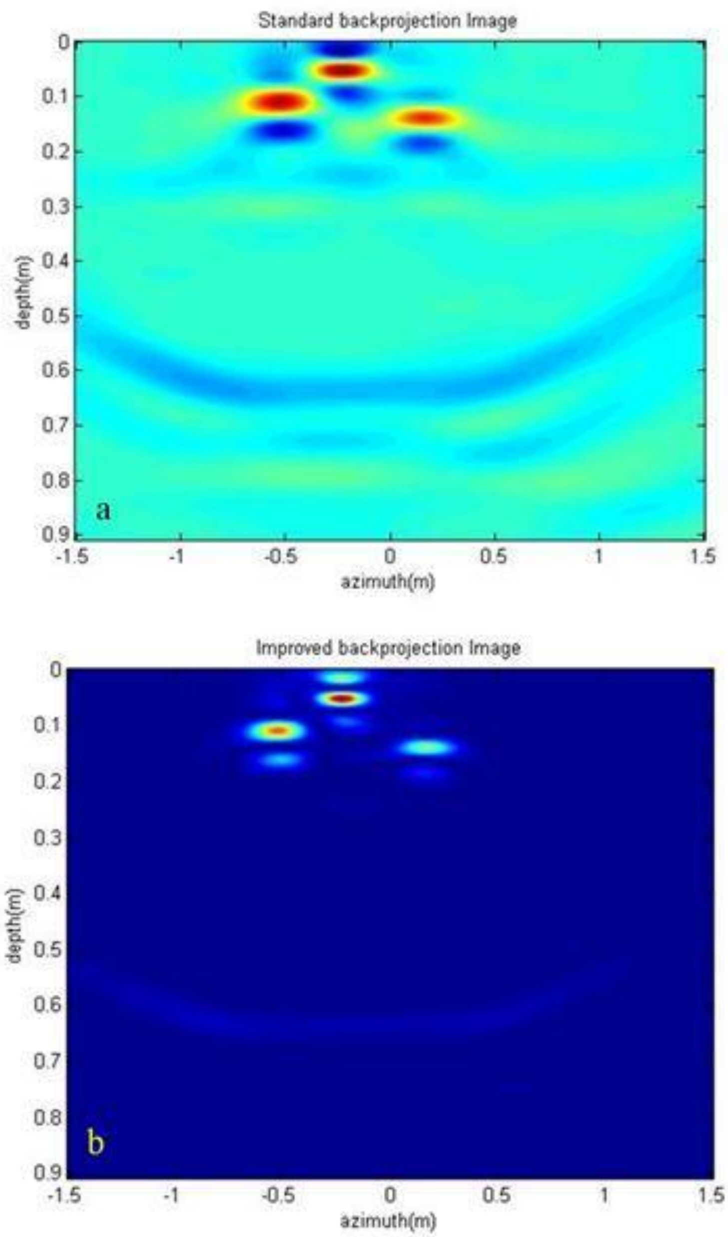

Figure 4: Comparison of imaging result for three landmines. (a) Result of the standard BP algorithm. (b) Result of the improved BP algorithm.

In order to quantitatively describe the effect of artifacts suppression with standard and improved BP algorithms, we evaluated Integrated Sidelobe Ratio (ISLR) parameter. This parameter is the ratio of the energy in the side-lobes to that contained in the main-lobe that is defined as follows:

Research Article

$$ISLR = 10\log\left(\frac{E_{side}}{E_{main}}\right) \qquad (13)$$

Where, E_{main} and E_{side} are the energy of main lobe of object and the energy of side lobe of object that is defined $(E_{total} - E_{main})$, and E_{total} is the energy of the image. The calculated ISLR parameter for Figure 5 (b) and (a) are -6.4446 dB and -3.8979 dB, respectively. The ISLR parameter decreases by $2.5467\ dB$.

For better understanding of the decrease and suppression of artifacts with standard and improved algorithms, two profiles at the peak point along y and depth axes of the imaging results are displayed in Figure 5. An average decline of suppression is 2.5 dB in both profiles that are shown in Figure 5(a) and (b).

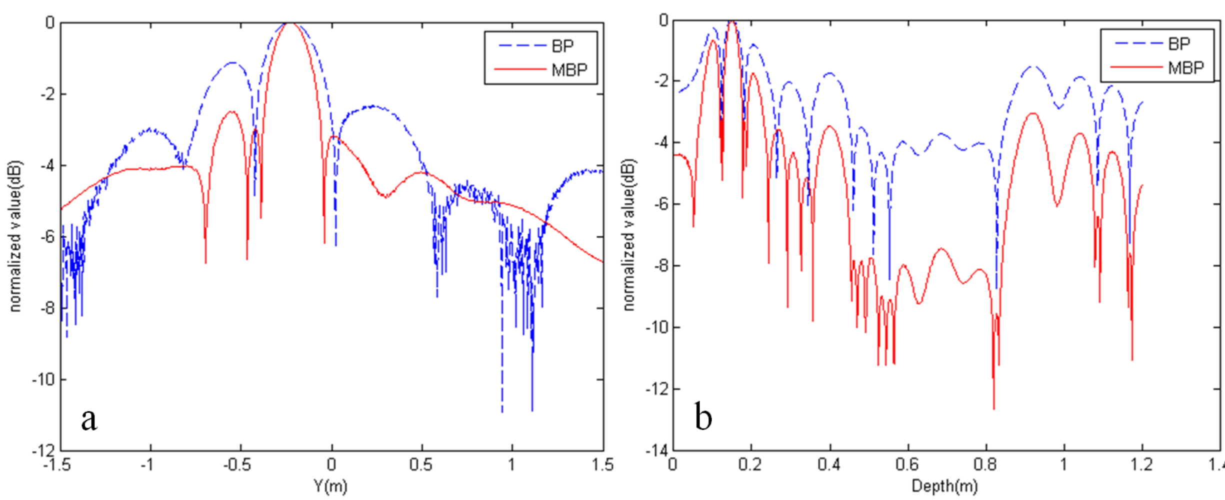

Figure 5: Comparison of profiles at the peak point. (a). Profile along y axis. (b) Profile along depth axis

Experimental Results

A GPR survey was conducted in order to test the standard and improved proposed BP imaging algorithm. The goal of this survey is imaging two buried metallic bars (PEC) in concrete block. The equipment evaluated in this study is a RAMAC/GPR (MALA Geosciences) and a shielded ground-coupled antenna with a nominal central frequency of 2.3 GHz. In this experiment, two identical iron bars were buried at nearly 10 and 13 cm below the homogeneous concrete block. The two metallic bars were put along the x-axis. The relative permittivity of concrete block was 4.5.

Under monostatic configuration, the backscattered field data were collected along a synthetic aperture with a length of 80 cm. Antenna was located just above the concrete surface and headed toward the buried object while moving along the aperture.

Assuming that the bars routes are generally known a-priori, the B-scan measurements along the longitudinal direction of the bars were taken. The acquired time series of B-scan data were then processed to locate the buried bars. Figure 6 shows the imaging result of GPR received data after preprocessing.

As expected, the imaging result was hyperbolically defocused due to different round-trip distances between targets and antennas while radar is moving along straight line for the mono-static arrangement.

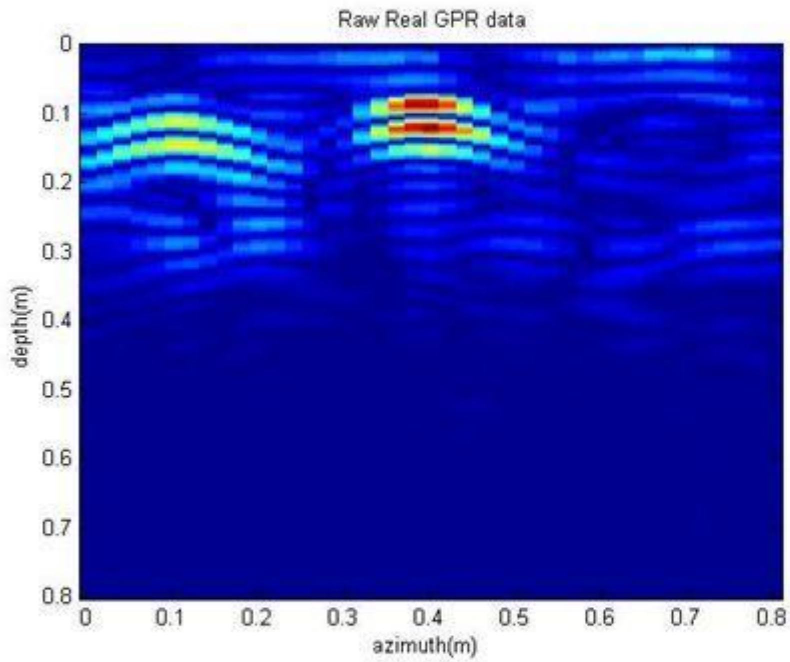

Figure 6: The Raw Real GPR image after pre-processing

Figure 7 shows the imaging result of standard and improved proposed BP algorithm, respectively. It is clear that Figure 7(a) has much more artifact than Figure 7(b). Obviously, image result from improved BP algorithm is more concentrated around the true location of the metallic bars and the reflection from other surfaces is well suppressed as they are not visible within the dynamic range of figure. Thus, superiority in artifact suppression and resolution of improved proposed BP algorithm over the standard one is conspicuous.

The calculated ISLR parameter for Figure 7(b) and (a) were -10.5527 dB and -8.3118 dB respectively and the ISLR parameter decreases by nearly $2.2409\ dB$.

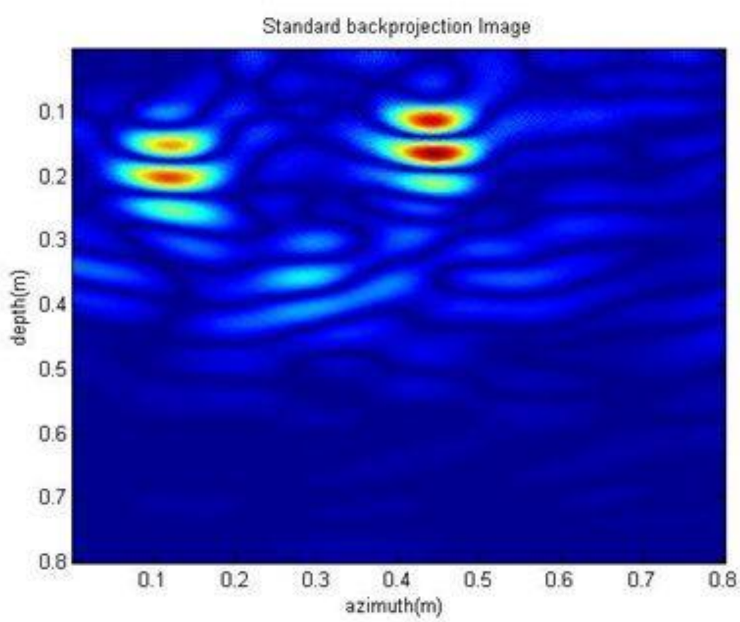

Indian Journal of Fundamental and Applied Life Sciences ISSN: 2231– 6345 (Online)
An Open Access, Online International Journal Available at www.cibtech.org/sp.ed/jls/2014/04/jls.htm
2014 Vol. 4 (S4), pp. 758-768/Akbari et al.
Research Article

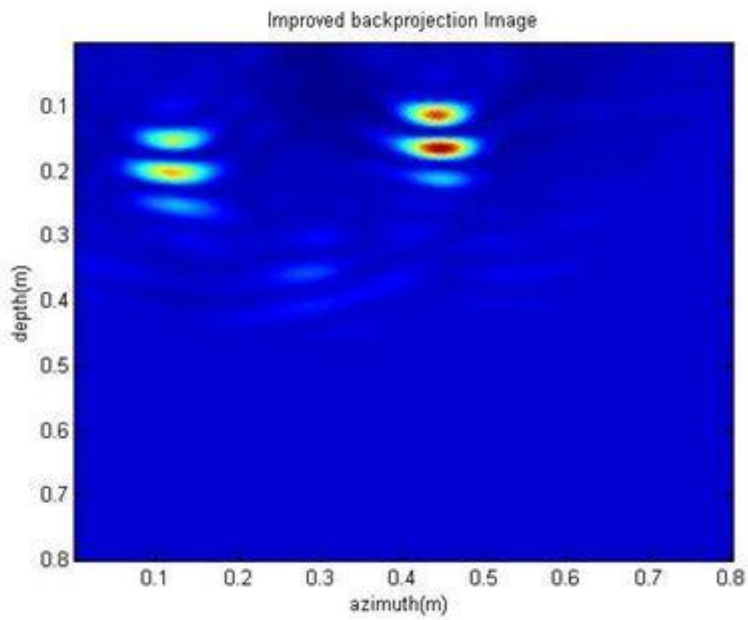

Figure 7: Comparison of imaging result for bars. (a) Result of the standard BP algorithm. (b) Result of the improved BP algorithm

For better understanding of the decrease and suppression of artifacts with standard and improved algorithms, two profiles at the peak point along y and depth axes of the imaging results are displayed in Figure 8. An average decline of suppression is 2.25 dB in both profiles that are seen in figure 8(a) and (b).

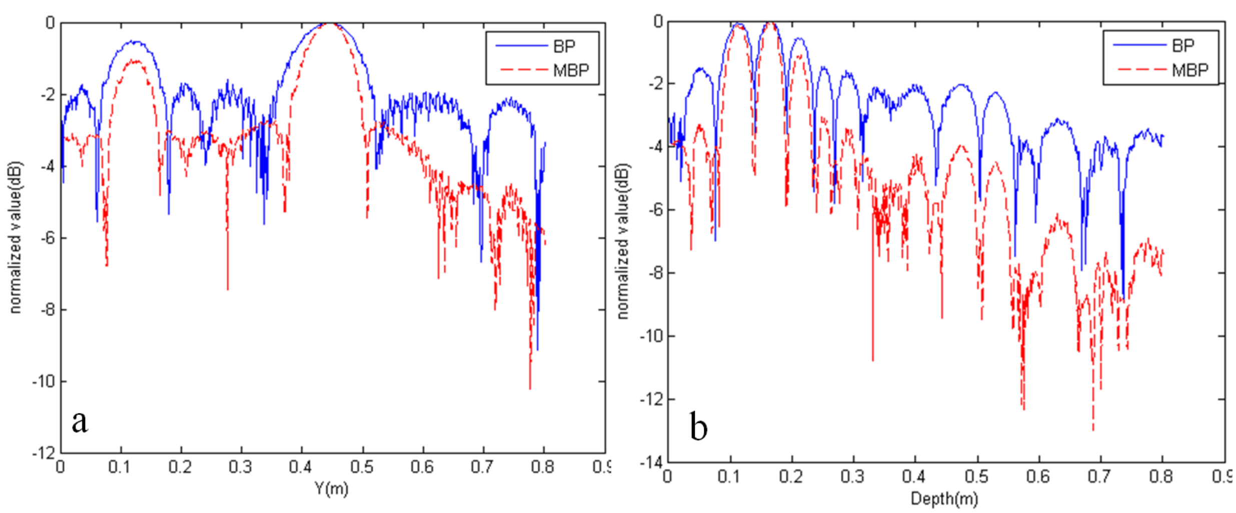

Figure 8: Comparison of profiles at the peak point. (a). Profile along y axis. (b) Profile along depth axis

CONCLUSION

This paper presented an improved version of the cross-correlation BP algorithm for GPR imaging. This improved proposed BP imaging algorithm has significantly suppressed noises and artifacts in the imaging result of the standard BP algorithm. By using a weight factor that designed by statistical character received data, imaging result showed a better performance for focusing quality. Simulation results and the real data imaging demonstrated its validity in GPR high resolution imaging. In order to quantitatively describe the imaging result for the effect of artifact suppression with proposed improved BP algorithm, a focusing parameter was evaluated. Future studies are recommended to focus on improving the proposed algorithm to adapt to disperse medium and multi-layer scenario.

REFERENCES

Carin L, Geng N, Sichina J and Nguyen L (1999). Ultrawide band synthetic aperture radar for mine-field detection. *IEEE Transactions on Antennas and Propagation* **41** 18-33.

Claerbout JF (1972). Downward continuation of moveout-corrected seismograms. *Geophysics* **37** 741–68.

Daniels DJ (2004). *Ground Penetrating Radar*, 2nd edition. (The Institution of Electrical Engineers: London, UK) IEE Radar, Sonar and Navigation Series 15, 1-19.

Fear EC, Li X, Hagness SC and Stuchly MA (2002). Confocal microwave imaging for breast cancer detection: Localization of tumors in three dimensions. *IEEE Transactions on Biomedical Engineering* **49** 812–822.

Foo S and Kashyap S (2004). Cross-correlated back projection for UWB radar imaging. In *Proceeding of IEEE Antennas Propagation Society International Symposium* 1275–1278.

Gazdag J (1978). Wave equation migration with the phase-shift method. *Geophysics* **43** 1342-51

Gu K, Wang G and Li J (2004). Migration based SAR imaging for ground penetrating radar systems. *Proceedings of Radar* **151** 317-325.

Lim HB, Nhung TT, Li EP, Thang ND and Confocal (2008). Microwave imaging for breast cancer detection: Delay-multiply-and-sum image reconstruction algorithm. *IEEE Transactions on Biomedical Engineering* **55** 1697-704.

Mast JE and Johansson EM (1994). Three-dimensional ground penetrating radar imaging using synthetic aperture time-domain focusing. *Advanced Microwave and Millimeter Wave Detectors* **2275** 205–214.

Miller C, Oristaglio M and Beylkin GA (1978). A new *slant on* seismic imaging*:* Migration integral geometry. *Geophysics* **52** 943-64.

Ozdemir C, Demirci S and Yigit E (2008). Practical algorithms to focus B-scan GPR images: theory and application to real data. *Progress In Electromagnetics Research B* **6** 109-22.

Ozdemir C, Lim S and Ling H (2004). A synthetic aperture algorithm for ground-penetrating Radar imaging. *Microwave and Optical Technology Letters* **42** 412-414.

Peters L, Daniels DJ and Young JD (1994). Ground penetrating radar as a subsurface environmental sensing tool. *Proceeding of IEEE* **82** 1802–1822.

Vitebskiy S, Carin L, Ressler MA and Le FH (1997). Short pulse ground penetrating radar: simulation and measurement. *IEEE Transactions on Geoscience and Remote Sensing* **35** 762-772.

Wiggins R (1985). Entropy guided deconvolution. *Geophysics* **50** 2720–2726.

Zetik R, Sachs J and Thoma R (2005). Modified cross-correlation back projection for UWB imaging: Numerical examples. In *Proceeding of IEEE International Conference Ultra-Wideband, Orlando, Florida, USA*, 11-15 July 650–654.